Phases in the system $Na_{1/2}Nd_{1/2}TiO_3$–$SrTiO_3$: a powder neutron diffraction study

2006 J. Phys.: Condens. Matter 18 9679

(http://iopscience.iop.org/0953-8984/18/42/014)

INSTITUTE OF PHYSICS PUBLISHING JOURNAL OF PHYSICS: CONDENSED MATTER

J. Phys.: Condens. Matter **18** (2006) 9679–9690 doi:10.1088/0953-8984/18/42/014

Phases in the system $Na_{1/2}Nd_{1/2}TiO_3$–$SrTiO_3$: a powder neutron diffraction study

Rajeev Ranjan[1,2], **Anupriya Agrawal**[3], **Anatoliy Senyshyn**[4,5] **and Hans Boysen**[1]

[1] Department für Geo- und Umweltwissenschaften, Sektion Kristallographie, Ludwig Maximillian Universität München, Am Coulombwall 1, 85748 Garching, München, Germany
[2] School of Materials Science and Technology, Institute of Technology, Banaras Hindu University, Varanasi-221005, India
[3] Department of Ceramic Engineering, Institute of Technology, Banaras Hindu University, Varanasi-221005, India
[4] Institute for Materials Science, Darmstadt University of Technology, Petersenstrasse 23, D-64287 Darmstadt, Germany
[5] Forschungsneutronenquelle Heinz Maier-Leibnitz (FRM II), Technical University München, 85748 Garching, Germany

Received 28 August 2006, in final form 17 September 2006
Published 6 October 2006
Online at stacks.iop.org/JPhysCM/18/9679

Abstract

A powder neutron diffraction study of $(Na_{1/2}Nd_{1/2})_{1-x}Sr_xTiO_3$ (NNST) has been carried out at room temperature. The system exhibits $Pbnm$ space group for $0 \leqslant x \leqslant 0.20$, $Ibmm$ space group for $0.30 \leqslant x \leqslant 0.40$, $I4/mcm$ space group for $0.50 \leqslant x \leqslant 0.80$ and $Pm\bar{3}m$ space group for $0.90 \leqslant x \leqslant 1.00$. The nature of these structural transitions is analysed in terms of the variation with composition of the lattice constants, octahedral tilting and strains. The results are discussed in the framework of group theoretical analysis of octahedral tilts in perovskites.

1. Introduction

The study of the evolution of crystallographic phases in perovskites, as a function of temperature, composition and pressure, is an area of continuing interest. Most of these structural transitions involve tilting and distortions of the anion octahedra in different ways, leading to a variety of structures [1–3]. The possible tilted perovskite structures have been classified in a systematic manner by Glazer [1, 2]. In this scheme of structure analysis, a distorted perovskite structure is considered as a superposition of octahedral tilts about the three pseudocubic axes. The tilts are of three types, namely zero (0), in-phase (+) and out-of-phase (−). A formal group theoretical analysis of this problem has shown that there are 15 distinct possible space groups for tilted octahedral structures. The in-phase (+) and the out-of-phase (−) tilts are associated with the irreducible representations, M_3^+ ($k = 1/2, 1/2, 0$) and R_4^+ ($k = 1/2, 1/2, 1/2$), respectively, of the space group $Pm\bar{3}m$.

The well known simplest tilt transition occurs in $SrTiO_3$ (ST). On cooling below 105 K, the structure changes from cubic (tilt system $a^0a^0a^0$, space group $Pm\bar{3}m$) to tetragonal (tilt system $a^0a^0c^-$, space group $I4/mcm$). This transition has been thoroughly investigated to understand the issues related to soft mode driven structural phase transitions in crystalline solids [4]. ST and $KTaO_3$ (KT) are also well known for their quantum paraelectric behaviour at low temperatures [5, 6]. Many more quantum paraelectric systems have subsequently been discovered [7–9]. The dielectric permittivity of the compounds exhibiting quantum paraelectricity increases on cooling but saturates below a certain temperature. It is believed that the zero point quantum fluctuations of the lattice prevent freezing of a soft ferroelectric mode and stabilize the paraelectric phase below the saturation temperatures [5]. Except for ST and KT, the saturation temperatures of the other quantum paraelectrics are comparatively higher and lie in the range 30 K $\leqslant T \leqslant$ 50 K. Because of the comparatively high saturation temperature, these compounds have also been termed as 'high temperature' quantum paraelectrics [8, 9]. It is interesting to note that the Curie–Weiss temperatures (T_c) of all the high temperature quantum paraelectrics are negative [8, 9]. In contrast, ST and KT exhibit positive values of T_c [5, 6]. Phenomenological theory of ferroelectric and antiferroelectric transitions can explain the positive and negative T_C values, respectively [10, 11]. This has led to speculation that the high temperature quantum paraelectrics may also be incipient antiferroelectric [12]. Stabilization of an antiferroelectric phase has been shown to occur in a related system $Sr_{1-x}Ca_xTiO_3$ [10, 11], a solid solution of compounds exhibiting 'low temperature' and 'high temperature' quantum paraelectric behaviour.

In this paper we report the evolution of structures in a solid solution of ST and $Na_{1/2}Nd_{1/2}TiO_3$ (NNT), another compound exhibiting high temperature quantum paraelectricity, using Rietveld analysis of powder neutron diffraction data. Since ST is cubic (space group $Pm\bar{3}m$) at room temperature, study of this series of solid solutions may help in understanding the phase transition behaviour of pure NNT on heating as it transforms to the most symmetric cubic structure. The present investigation is the first step towards establishing the complete phase diagram of this solid solution.

2. Experimental details

Solid solutions of NNT and ST were synthesized by the conventional solid state reaction method. Powders of Na_2CO_3, Nd_2O_3, $SrCO_3$, and TiO_2, each of purity higher than 99.5%, were thoroughly mixed in stoichiometric ratio in a ball mill with zirconia jars and zirconia balls. Acetone was used as a mixing medium. The mixed powders were calcined at 1000 °C for 3 h and were cold compacted before sintering at 1300 °C in air for 3 h. Sintered pellets were crushed to fine powders and annealed at 800 °C for ∼12 h to remove strains, possibly induced during the crushing process. The sintered powders were checked for their phase purity using a 18 kW Rigaku rotating anode x-ray powder diffractometer with copper target and a graphite monochromator in the diffracted beam. Neutron powder diffraction data were collected at structure powder diffractometer SPODI at the FRM-II research reactor, Germany [13], using a wavelength of 1.548 Å.

3. Results

Figure 1 shows magnified powder neutron diffraction patterns of some representative NNST compositions in a limited two theta range. The patterns are indexed with respect to a doubled pseudocubic cell of the type $2a \times 2b \times 2c$ to reveal the types of superlattice reflections. The

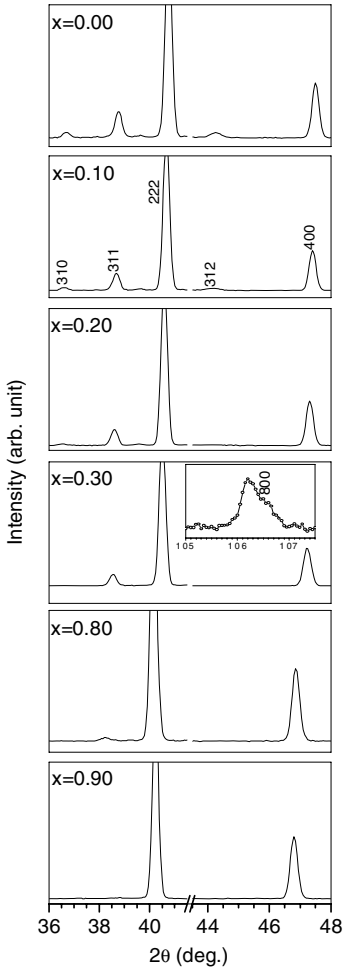

Figure 1. Neutron powder diffraction patterns of some representative compositions of $(Na_{1/2}Nd_{1/2})_{1-x}Sr_xTiO_3$ in the 2θ range 36.6°–48°.

patterns in the composition range $0 \leqslant x \leqslant 0.20$ exhibit superlattice reflections which are of 'all-odd (ooo)', and 'two-odd one even (ooe)' type indices, indicating the presence of out-of-phase (−) and in-phase (+) tilted octahedra, respectively, in the structure. Recently, we have shown that the structure of NNT at room temperature is consistent with $a^-a^-c^+$ tilt system and $Pbnm$ space group [14]. In view of this, the structure refinement for the compositions $0 \leqslant x \leqslant 0.20$ was carried out in the $Pbnm$ space group. Rietveld refinement was carried out using the software package Fullprof [15]. To model the peak profile shape, the pseudo-Voigt function has been chosen. The background contribution has been determined using a linear interpolation between selected data points in non-overlapping regions. The scale factor, zero angular shift, profile shape parameters, half width (Caglioti) parameters, asymmetry and lattice parameters as well as fractional coordinates of atoms and their isotropic thermal parameters were varied during the fitting. Figure 2 shows the Rietveld plot of $x = 0.10$ after the final cycle of structure refinement in the $Pbnm$ space group. The corresponding refined structural parameters along with the R-factors are given in table 1.

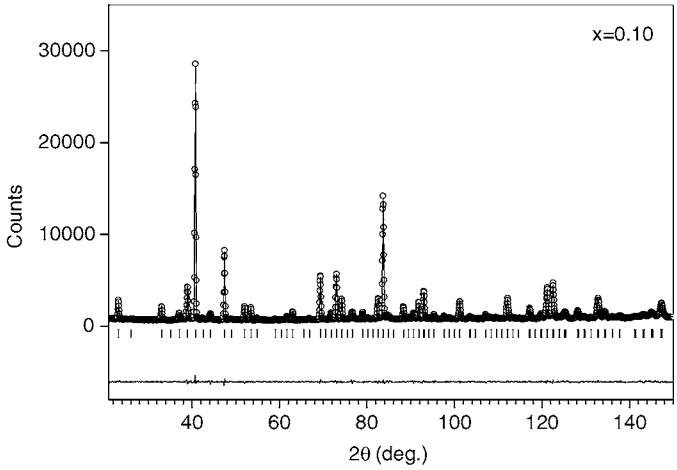

Figure 2. Observed (open circles), calculated (continuous line) and difference (continuous line near the bottom) plots after the final refined cycle in the $Pbnm$ space group for $x = 0.10$. The vertical bars indicate positions of the Bragg peaks.

For the compositions $x \geqslant 0.30$, the ooe type superlattice reflections are absent. The remaining ooo reflections persist until $x = 0.80$ above which they also vanish, suggesting a transition to cubic perovskite structure with space group $Pm\bar{3}m$. A perusal of the tilt systems suggests that there are five space groups, namely $F\bar{1}$, $I2/a$, $Ibmm$, $I4/mcm$ and $R3c$, with only negative tilts [1–3]. For a rhombohedrally distorted structure, one would expect the $h00$ pseudocubic reflections to remain singlet, while the hhh pseudocubic reflections split into two. However, the fact that the pseudocubic reflection, 400 (in the figure it is indexed as 800 to maintain consistency of the indexing with respect to the doubled pseudocubic cell), near $2\theta = 106°$ is not a singlet (see inset of $x = 0.30$ in figure 1) proves that the structure of $x = 0.30$ cannot be rhombohedral. Refinement in the space group $F\bar{1}$ was not attempted. To determine the correct structures of the various compositions in the range $0.30 \leqslant x \leqslant 0.80$, results of structure refinements in the remaining three space groups, $I2/a$, $Ibmm$, and $I4/mcm$ were compared. The refinement was carried out in the order of decreasing space group symmetry. Figure 3(a) depicts the Rietveld plot for $x = 0.30$ after refining the structure in the $I4/mcm$ space group. The goodness of fit, χ^2, was obtained as 3.32. Although the fit between the observed and the calculated profiles is reasonably good at angles lower than 100°, one observes increasing misfit at higher angles. The inset in figure 3(a) clearly reveals the inadequacy of the space group $I4/mcm$ to explain the observed superlattice reflection near 145°, whose index with respect to the doubled pseudocubic cell is 931. In view of this, structure refinement was carried out in the next lower symmetry space group, $Ibmm$. This led to a decrease in χ^2 value to 2.18. The corresponding Rietveld plot is shown in figure 3(b). As is evident from the inset of this figure, the calculated Bragg profile reasonably accounts for the features of the observed Bragg reflection near 145°. No further improvement in the fit was obtained when refined in the monoclinic space group. This was also true for the composition $x = 0.40$. We therefore conclude that the correct space group for $x = 0.30$ and 0.40 is $Ibmm$ corresponding to $a^-a^-c^0$ tilt system.

For $0.50 \leqslant x \leqslant 0.80$, the minimum value of χ^2 was found to be identical for both, $I4/mcm$ and $Ibmm$, space groups. In fact, it was found that for $x = 0.80$, the goodness of fit oscillates when refinement was carried out in the $Ibmm$ space group, particularly when the

Table 1. Refined structural parameters of $(Na_{1/2}Nd_{1/2})_{1-x}Sr_xTiO_3$.

		$x = 0.0$ *Pbnm*	$x = 0.1$ *Pbnm*	$x = 0.2$ *Pbnm*	$x = 0.3$ *Ibmm*	$x = 0.4$ *Ibmm*	$x = 0.5$ *I*4/*mcm*	$x = 0.6$ *I*4/*mcm*	$x = 0.7$ *I*4/*mcm*	$x = 0.8$ *I*4/*mcm*	$x = 0.9$ $Pm\bar{3}m$
Na–Nd/Sr	*x*	−0.002(2)	−0.003(2)	0.002(2)	−0.0018(9)	−0.004(1)	0.00	0.00	0.00	0.00	0.00
	y	0.5097(7)	0.5058(8)	0.501(1)	0.50	0.50	0.50	0.50	0.50	0.50	0.00
	z	0.25	0.25	0.25	0.25	0.25	0.25	0.25	0.25	0.25	0.00
	B (Å^2)	0.86(3)	0.80(3)	0.76(3)	0.70(3)	0.67(2)	0.51(2)	0.33(2)	0.46(2)	0.44(2)	0.46(2)
Ti	*x*	0.00	0.00	0.00	0.00	0.00	0.00	0.00	0.00	0.00	0.50
	y	0.00	0.00	0.00	0.00	0.00	0.00	0.00	0.00	0.00	0.50
	z	0.00	0.00	0.00	0.00	0.00	0.00	0.00	0.00	0.00	0.50
	B (Å^2)	0.64(4)	0.62(4)	0.57(5)	0.35(4)	0.36(4)	0.22(3)	0.17(3)	0.21(4)	0.25(4)	0.12(3)
O1	*x*	−0.0607(7)	−0.0555(8)	−0.0534(6)	−0.0465(5)	−0.0391(5)	0.00	0.00	0.00	0.00	0.50
	y	−0.0064(8)	−0.003(1)	0.003(2)	0.00	0.00	0.00	0.00	0.00	0.00	0.50
	z	0.25	0.25	0.25	0.25	0.25	0.25	0.25	0.25	0.25	0.00
	B (Å^2)	0.72(5)	0.71(5)	0.69(6)	0.77(5)	0.96(6)	1.51(6)	0.85(6)	0.81(7)	0.49(8)	0.53(2)
O2	*x*	0.2246(4)	0.2291(5)	0.2376(7)	0.25	0.25	0.2238(2)	0.2272(2)	0.2315(2)	0.2360(2)	
	y	0.2752(4)	0.2716(4)	0.2629(7)	0.25	0.25	0.2762(2)	0.2728(2)	0.2685(2)	0.2640(2)	
	z	0.0321(3)	0.0305(3)	0.0280(3)	0.0262(2)	0.0242(3)	0.00	0.00	0.00	0.00	
	B (Å^2)	0.99(4)	1.08(4)	1.14(4)	1.07(3)	1.02(3)	0.51(2)	0.44(2)	0.62(3)	0.60(4)	
	a (Å)	5.4378(2)	5.4511(2)	5.4637(2)	5.4764(2)	5.4846(3)	5.4836(1)	5.4919(1)	5.5006(1)	5.5089(1)	3.90187(3)
	b (Å)	5.4448(2)	5.4534(2)	5.4629(2)	5.4705(2)	5.4778(2)					
	c (Å)	7.6921(3)	7.7049(3)	7.7142(2)	7.7236(2)	7.7340(3)	7.7725(3)	7.7887(3)	7.7966(3)	7.8006(3)	
	R_p	4.25	3.92	4.77	3.63	4.03	3.92	4.48	5.27	4.83	4.75
	R_{wp}	5.47	5.23	6.23	4.94	5.24	5.23	5.93	7.09	6.64	6.63
	R_e	2.92	3.13	3.48	3.34	3.18	3.34	4.38	4.62	4.56	3.32
	χ^2	3.51	2.79	3.20	2.18	2.72	2.45	1.83	2.35	2.12	3.9

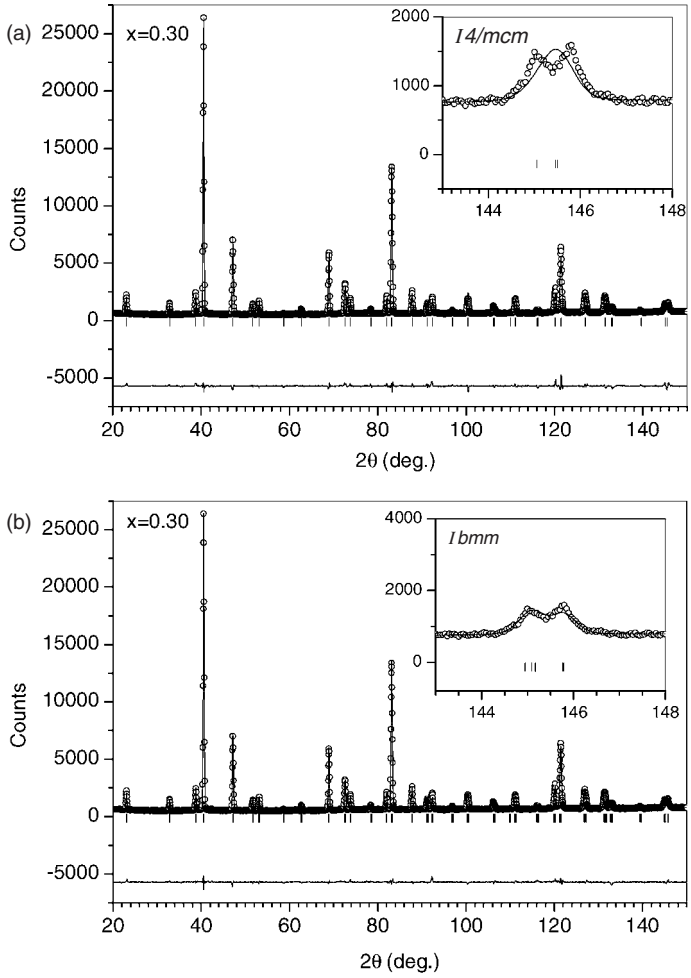

Figure 3. Observed (open circles), calculated (continuous line) and difference (continuous line near the bottom) plots for $x = 0.30$ after the final refined cycle in the (a) $I4/mcm$ and (b) $Ibmm$ space groups. The vertical bars indicate positions of the Bragg peaks.

lattice parameters were refined. Thus $I4/mcm$ is accepted as the correct space group for these compositions. Another feature that confirms our conclusion is the fact that the reduced cell parameter c_p is less than a_p/b_p for $x < 0.50$ and becomes greater than a_p/b_p for $x \geqslant 0.50$ (see figure 6(a)). This fits well with the predictions of Glazer according to which a structure with tilt system $a^-a^-c^0$ should have the subcell parameter c less than either of a or b, while a structure with $a^0a^0c^-$ tilt system should have c greater than a/b [1, 2]. Figure 4 shows the Rietveld plot for $x = 0.50$ obtained after the final cycle of refinement. For the sake of completeness, we have also refined the structure of $x = 0.90$, with $Pm\bar{3}m$ space group (see figure 5). The refined structural parameters of all the compositions are given in table 1.

The variation of the reduced cell parameters (a_p, b_p, c_p), obtained from the orthorhombic/tetragonal lattice parameters $(a_o/a_t\ b_o/b_t\ c_o/c_t)$ using the relationships $a_o/a_t = \sqrt{2}a_p$, $b_o/b_t = \sqrt{2}b_p$, and $c_o/c_t = 2c_p$, and also the unit cell volume are plotted in figure 6. It is evident from this figure that the differences in the a, b and c parameters throughout the

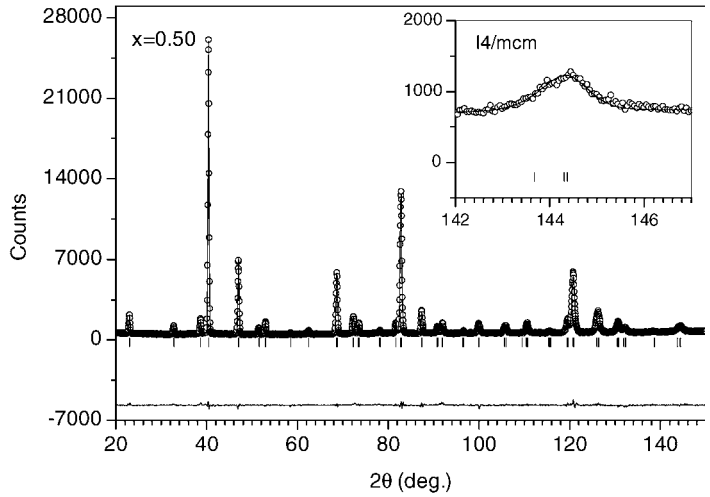

Figure 4. Observed (open circles), calculated (continuous line) and difference (continuous line near the bottom) plots after the final refined cycle in the $I4/mcm$ space group for $x = 0.50$. The vertical bars indicate positions of the Bragg peaks.

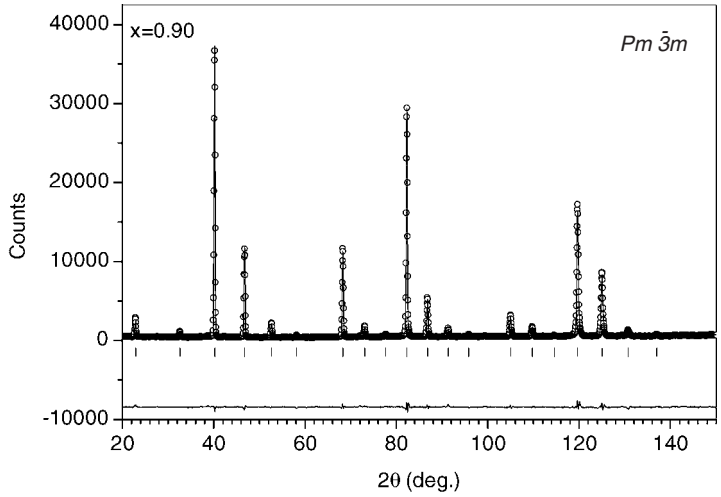

Figure 5. Observed (open circles), calculated (continuous line) and difference (continuous line near the bottom) plots after the final refined cycle in the $Pm\bar{3}m$ space group for $x = 0.90$. The vertical bars indicate positions of the Bragg peaks.

composition range are less than 0.02 Å, suggesting very weak distortion of the cubic lattice. This fact is manifested in the powder patterns as weak splittings of some of the main Bragg reflections only at angles greater than 100°. At low angles (<100°), the Bragg peaks appear as a singlet.

The lattice parameters and cell volume increases with increasing x (see figure 6(a)). This is consistent with the fact that the Shannon radius (for CN:12) of Sr^{2+} (1.44 Å) is larger than the average Shannon radius of $Na_{1/2}Nd_{1/2}$ (1.33 Å) for the same coordination [16]. It is, however, interesting to note that the orthorhombic a- and b-parameters intersect near $x = 0.20$,

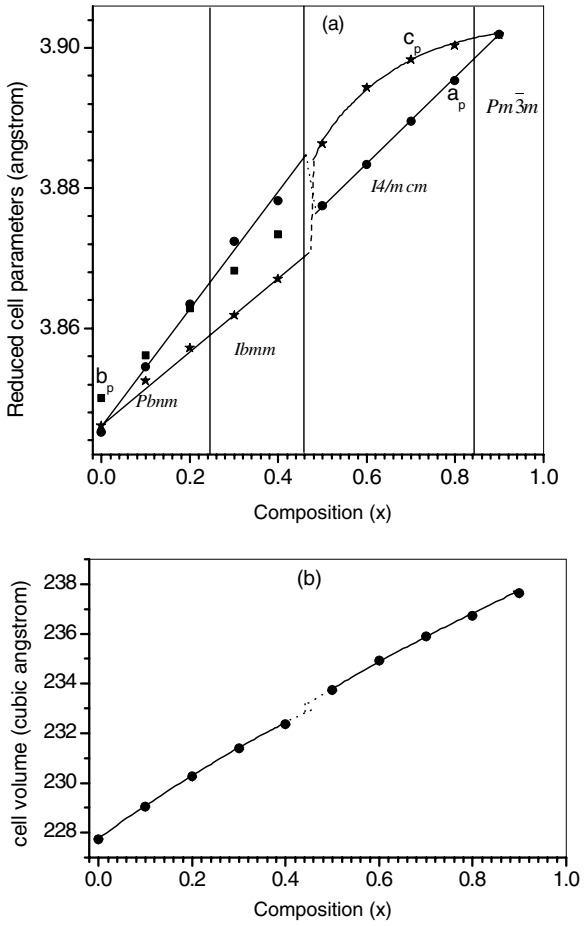

Figure 6. Variation of (a) reduced cell parameters, a_p (filled circles), b_p (filled squares), c_p (filled stars) and (b) unit cell volume of $(Na_{1/2}Nd_{1/2})_{1-x}Sr_xTiO_3$ with composition. Lines are guides to eyes. The discontinuities are marked with dashed and dotted lines.

suggesting that the lattice exhibits a pseudo-tetragonal distortion around this composition. This, however, is accidental since in the classification scheme of tilted perovskite structures there is no possibility of a tetragonal structure with superposed in-phase and out-of-phase tilted octahedra. Another interesting feature is discontinuities in the a- and c-parameters across $0.40 < x < 0.50$. The a-parameter decreases, while the c-parameter exhibits a discontinuous increase across this composition. The unit cell volume also exhibits a very weak but distinct discontinuity across this composition boundary (figure 6(b)).

Figure 7 depicts the variation of both the octahedral tilt angles, in-phase (+) and out-of-phase (−), corresponding to the irreducible representations (IRs) M_3^+ and R_4^+, respectively, as a function of composition. The octahedral tilt angles were derived from the location of the equatorial oxygen O_2 at $1/4 - u$, $1/4 + v$, w [17]. The in-phase tilt angle (φ) around [001] of the parent cubic phase is given by $\tan\varphi = 2(u + v)$. Since structures in the $Pbnm$ and $Ibmm$ space groups correspond to $a^-a^-c^+$ and $a^-a^-c^0$ tilt systems, the composite out-of-phase tilt angle (ψ) is determined about the [110] of the cubic parent structure using the relation: $\tan\psi = 4\sqrt{2}w$. In principle, if the octahedra are not distorted, the same value of ψ

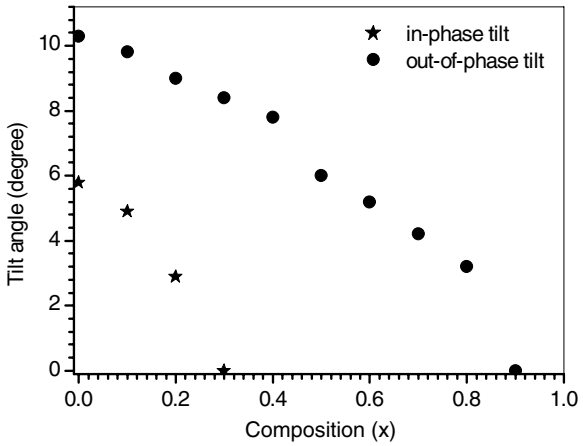

Figure 7. Variation of in-phase (φ) and out-of-phase (ψ) tilt angles with composition. ψ is calculated about the [110] direction of the parent cubic cell for $x < 0.50$ using the relation $\tan\psi = 4\sqrt{2}w$ and about the [001] direction of the parent cubic cell for $x \geqslant 0.50$ (see text).

should be obtained using the relationship: $\tan\psi = -2\sqrt{2}x(\mathrm{O1})$. Differences in the values calculated using the two formulae would then indicate octahedral distortion. For the structure corresponding to the $I4/mcm$ space group, the out-of-phase tilt about [001] is determined in the way discussed above for the in-phase tilt. However, in this case, the space group symmetry constrains the magnitudes of u and v to be equal. The tilt angles are maximum for $x = 0.00$ with values $\varphi = 5.8°$ and $\psi = 10.3°$ (obtained using the expression $\tan\psi = 4\sqrt{2}w$). The corresponding value of ψ obtained using the expression: $\tan\psi = -2\sqrt{2}x(\mathrm{O1})$ is 9.7°. Considering the fact that error in its measurement can be ∼0.3°, the difference, 0.6°, is not very significant. The oxygen octahedra can therefore be treated as nearly regular for $x = 0.00$. A detailed analysis of octahedral distortion as a function of composition is presented in the next paragraph. Predictably, since $SrTiO_3$ exhibits untilted octahedra at room temperature, the tilt angles in NNST decrease with increasing Sr content (see figure 7). With increasing Sr concentration, the in-phase tilt first vanishes somewhere in the range $0.20 < x \leqslant 0.30$ followed by vanishing of the out-of-phase tilt for $x > 0.80$. This sequence of disappearance of tilt angles is a common feature in most of the orthorhombic perovskites.

The phase transitions mentioned above are also marked by anomalous behaviour of the octahedral parameters. Figure 8(a) shows the variation of the mean Ti–O bond length as a function of composition. It is interesting to note that the variation of mean Ti–O bond length exhibits a nonmonotonic behaviour. The values first decrease till $x = 0.30$, remain almost constant for $x = 0.40$, and then increase with increasing x beyond $x = 0.40$. The initial decrease in the mean Ti–O bond length is marked with an increase in the distortion of the oxygen octahedra. Octahedral distortion was estimated by measuring the difference between the maximum and minimum Ti–O bond lengths. For regular octahedra, e.g. in $SrTiO_3$, this value is zero. Despite the fact that $SrTiO_3$ is known to exhibit cubic structure with regular undistorted octahedra, the initial substitution of Sr in NNT increases the octahedral distortion (see figure 8(b)). This can be attributed to the fact that with increasing x the system is driven towards a lattice instability. The first instability occurs at $x = 0.30$ whence the transition to $Ibmm$ structure takes place. The octahedron is relatively regular in this phase as evidenced by a sharp decrease of the octahedral distortion. The next lattice instability corresponding to the transition to tetragonal ($I4/mcm$) structure at $x = 0.50$ is again accompanied by enhancement

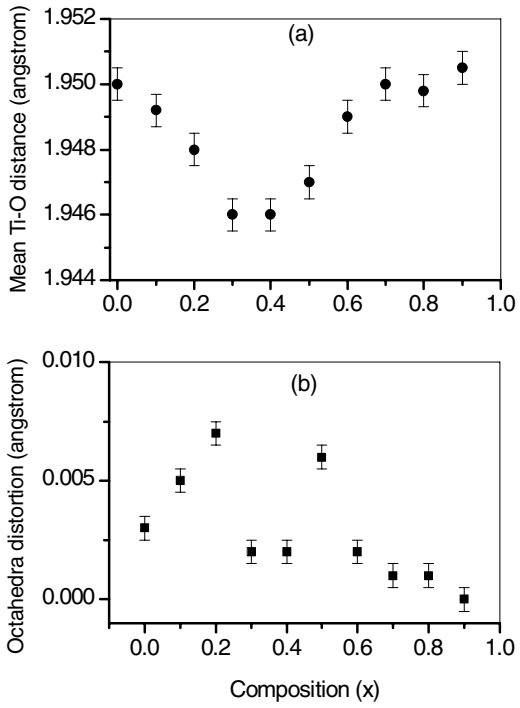

Figure 8. Variation of (a) mean Ti–O bond distance and (b) octahedral distortion (maximum Ti–O distance − minimum Ti–O distance) with composition.

of octahedral distortion. For $x > 0.50$, the octahedral distortion gradually decreases and becomes zero as the composition approaches $x = 1.00$ without exhibiting any anomalous variation across the $I4/mcm$–$Pm\bar{3}m$ transition.

4. Discussion

From the foregoing, it is clear that the system NNST exhibits two intermediate phases, $Ibmm$ and $I4/mcm$, with increasing Sr content, apart from the structures of the parent compounds with space groups $Pbnm$ and $Pm\bar{3}m$.

Orthorhombic	→	orthorhombic	→	tetragonal	→	cubic
$Pbnm(a^-a^-c^+)$		$Ibmm(a^-a^-c^0)$		$I4/mcm(a^0a^0c^-)$		$Pm\bar{3}m(a^0a^0a^0)$.

The two intermediate structures, $Ibmm$ and $I4/mcm$ are closely related and it was possible to identify the correct one, i.e. $Ibmm$ for $x = 0.30$ and 0.40, only through Rietveld analysis of Bragg reflections at large 2θ angles (e.g. the reflection at 145°). At such large angles the Bragg reflections become extremely weak in x-ray diffraction data. Laboratory XRD data can therefore be of no help to resolve such a subtle difference.

It would be interesting to investigate the system at close composition intervals in the crossover domain $0.4 < x < 0.5$ for understanding the composition dependence of the nature of the $Ibmm$–$I4/mcm$ phase transition. Viewed from the $SrTiO_3$ side, it is well known that pure $SrTiO_3$, which is cubic at room temperature, undergoes an antiferrodistortive phase transition to a tetragonal ($I4/mcm$ space group) structure below 105 K. This transition is driven by freezing of one of the triply degenerate soft phonons, R_4^+, at the R point of the

cubic Brillouin zone. The freezing temperature of this phonon can be raised by chemical substitution and the tetragonal structure stabilized at room temperature or above. Substitution of $Na_{1/2}Nd_{1/2}$ (NN) at the Sr site seems to do precisely the same by stabilizing the $I4/mcm$ structure at room temperature for compositions below $x = 0.90$. Although $I4/mcm$ structures persist till $x = 0.50$, it is noted that the thermal parameter of the apical oxygen, O1, is higher (1.51 $Å^2$) than the values for the other compositions (max value = 0.96 $Å^2$ for $x = 0.40$). The relatively large B could be due to the proximity of this composition to the $Ibmm$–$I4/mcm$ phase boundary. In the orthorhombic ($Ibmm$) structure, oxygen O1 can take up an off-centre position along the x-axis of the orthorhombic cell. This is not so in the $I4/mcm$ structure. The large thermal parameter of O1 for $x = 0.50$ seems to be suggestive of a precursor effect of transition from the tetragonal ($I4/mcm$) structure to the orthorhombic ($Ibmm$) structure.

Viewed from the $SrTiO_3$ side, composition variation of the c_p of NNST exhibits a trend (see figure 6) which is similar to that reported for $Sr_{1-x}Ca_xTiO_3$ (SCT) [18]. However, in the case of SCT, it has been shown that the sharp drop in the c-parameter for $x > 0.35$ is related to the transition to an antiferroelectric phase which is stable at room temperature only for a narrow composition range $0.35 < x < 0.41$ [18]. The space group of the antiferroelectric phase has been reported to be $Pbcm$ and the structure is isostructural with the P phase of $NaNbO_3$ [19]. One characteristic feature of this antiferroelectric structure is that the c-axis of the orthorhombic cell is nearly four times the pseudocubic subcell length. It would be interesting to look for a similar kind of phase in NNST by careful analysis of the diffraction patterns at close composition intervals in the range $0.40 < x < 0.50$.

It is worthwhile considering the sequence of transitions mentioned above in the light of Landau theory of phase transitions [3]. As per this analysis, the first transition, i.e. $Pbnm$–$Ibmm$, is allowed to be continuous. The same is also true for the $Pm\bar{3}m$–$I4/mcm$ transition. However, the $Ibmm$–$I4/mcm$ transition is predicted to be of discontinuous nature. This correlates very well with the discontinuous jumps in the lattice parameters that occur across $0.40 < x < 0.50$. Because of its first-order nature, coexistence of the two phases is likely to occur in a certain composition range at room temperature. The features corresponding to the coexistence of $Ibmm$–$I4/mcm$ may be experimentally difficult to determine using powder diffraction techniques since the sets of superlattice reflections are identical for both the structures, and the distortions of the subcell from the parent cubic is very weak. Raman scattering techniques can, however, reveal such features unambiguously. Temperature dependent studies of the compositions exhibiting $Ibmm$ and $I4/mcm$ structures at room temperature may be more helpful in unravelling the features associated with the $Ibmm$–$I4/mcm$ transition.

The sequence of transitions observed for NNST has also been reported in temperature dependent studies for $SrZrO_3$ [20], $SrRuO_3$ [21] and in composition studies on the systems $Sr_{1-x}Ba_xSnO_3$ [22] and $Sr_{1-x}Ba_xHfO_3$ [23], suggesting that this sequence of transitions is a common feature of many of the orthorhombic perovskites.

5. Conclusions

The solid solution of $(Na_{1/2}Nd_{1/2})_{1-x}Sr_xTiO_3$ exhibits the following sequence of structures on increasing x: $Pbnm$–$Ibmm$–$I4/mcm$–$Pm\bar{3}m$. The structure change, $Ibmm$–$I4/mcm$, across $0.40 < x < 0.50$ is marked with a small discontinuous jump in the lattice parameters, suggesting a first-order nature of this transition. No such discontinuity is seen across the $Pbnm$–$Ibmm$ and $I4/mcm$–$Pm\bar{3}m$ transitions. The results are consistent with the group theoretical analysis of phase transitions in perovskites.

Acknowledgment

RR is grateful to the von Alexander Humboldt Foundation for the award of a fellowship for this work.

References

[1] Glazer A M 1972 *Acta Crystallogr.* B **28** 3384
[2] Glazer A M 1975 *Acta Crystallogr.* A **31** 756
[3] Howard C J and Stokes H T 2005 *Acta Crystallogr.* A **61** 93
[4] Cowley R A 1980 *Adv. Phys.* **29** 1
[5] Muller K A and Burkard H 1979 *Phys. Rev.* B **19** 3593
[6] Samara G A and Morosin B 1973 *Phys. Rev.* B **8** 1256
[7] Kim I S, Itoh M and Nakamura T 1992 *J. Solid State Chem.* **101** 77
[8] Sun P H, Nakamura T, Shan Y J, Inaguma Y and Itoh M 1997 *Ferroelectrics* **200** 93
[9] Shan Y J, Nakamura T, Inaguma Y and Itoh M 1998 *Solid State Ion.* **108** 123
[10] Ranjan R, Pandey D and Lalla N P 2000 *Phys. Rev. Lett.* **84** 8726
[11] Ranjan R and Pandey D 2001 *J. Phys.: Condens. Matter* **13** 4239
[12] Chandra A, Ranjan R, Singh D P, Khare N and Pandey D 2006 *J. Phys.: Condens. Matter* **18** 2977
[13] Gilles R, Krimmer B, Boysen H and Fuess H 2002 *Appl. Phys.* A **74** S148
[14] Ranjan R, Agrawal A, Senyshyn A and Boysen H 2006 *J. Phys.: Condens. Matter* **18** L515
[15] Rodrigues-Carvajal J 2000 *FULLPROF. A Rietveld Refinement and Pattern Matching Analysis Program* Laboratoire Leon Brillouin (CEA-CNRS), France
[16] Shannon R D 1976 *Acta Crystallogr.* A **32** 751
[17] Kennedy B J, Howard C J and Chakoumakos B C 1999 *J. Phys.: Condens. Matter* **11** 1479
[18] Ranjan R, Pandey D, Schuddinck W, Richard O, Meulenaere P De, Landuyt J V and Tendeloo G V 2001 *J. Solid State Chem.* **162** 20
[19] Cowley A C S, Lukaszewicz K and Megaw H D 1969 *Acta Crystallogr.* B **25** 851
[20] Howard C J, Knight K S, Kennedy B J and Kisi E H 2000 *J. Phys.: Condens. Matter* **12** L677
[21] Kennedy B J, Hunter B A and Hester J R 2002 *Phys. Rev.* B **65** 224103
[22] Mountstevens E H, Attfield J P and Redfern S A T 2003 *J. Phys.: Condens. Matter* **15** 8315
[23] Li L, Kennedy B J, Kubota Y, Kato K and Garrett R F 2004 *J. Mater. Chem.* **14** 263